

Senescence in neural cell lines: comparative insights from SH-SY5Y and ReNcell VM

Kristina Macova^{1,2}, Diana Mjartinova^{1,3}, Lubica Fialova¹, Dalibor Nakladal⁴  and Dominika Fricova^{1,4,5}

¹ *Institute of Neuroimmunology, Slovak Academy of Sciences, Bratislava, Slovakia*

² *Faculty of Natural Sciences, Department of Molecular Biology, Comenius University in Bratislava, Bratislava, Slovakia*

³ *Faculty of Medicine, Comenius University in Bratislava, Bratislava, Slovakia*

⁴ *Comenius University Science Park, Clinical Research Unit, Bratislava, Slovakia*

⁵ *Unit for translational research of neurodegenerative diseases, 2nd Neurology Department, Faculty of Medicine and University Hospital Bratislava, Comenius University in Bratislava, Bratislava, Slovakia*

Abstract. Senescence, a crucial yet paradoxical phenomenon in cellular biology, acts as a barrier against cancer progression while simultaneously promoting aging and age-related pathologies. This duality underlines the importance of precise monitoring of senescence response, especially with regard to the proposed use of drugs selectively removing senescent cells. In particular, little is known about the role of senescence in neurons and in neurodegenerative diseases. Our study investigates the senescence response in neuroblastoma SH-SY5Y cells and human neural progenitor ReNcell VM cells exposed to doxorubicin, a chemotherapeutic agent known to induce DNA damage and subsequent senescence. Through a comprehensive analysis employing the most robust senescence markers, we characterized the senescence-associated patterns in these neural cell lines including cellular morphological changes, SA-beta-gal, γ H2A.X, p21^{Waf1/Cip1} and p16^{Ink4a}. Our findings indicate that ReNcell VM cells exhibit greater senescence-associated response at lower doxorubicin concentrations compared to SH-SY5Y cells. Additionally, we observed cell-type-specific differences in timing and levels of the expression of key cell cycle regulators during senescence. Our results emphasize the necessity of cell-type-specific strategies in senescence research with regard to implications as well as limitations for translation into aging and neurodegenerative disorders.

Key words: Senescence — Neural cells — Doxorubicin — p16^{Ink4a} — p21^{Waf1/Cip1}

Highlights

- For the first time, we comprehensively described senescence induction-associated changes in neural model cell line ReNcell VM commonly used for neurobiological studies.
- In our study, we discovered that ReNcell VM cells undergo senescence at lower doses of doxorubicin compared to SH-SY5Y cells. Additionally, we found that the timing of the senescence response varies between the two cell lines, with ReNcell VM cells exhibiting a more rapid onset of senescence markers. This differential sensitivity and response timing highlight the unique cellular dynamics of senescence in these neural models.

Correspondence to: Dominika Fricova, Institute of Neuroimmunology, Slovak Academy of Sciences, Bratislava, 84510, Slovakia
E-mail: fricova1@uniba.sk

© The Authors 2025. This is an **open access** article under the terms of the Creative Commons Attribution-NonCommercial 4.0 International License (<https://creativecommons.org/licenses/by-nc/4.0/>), which permits non-commercial use, distribution, and reproduction in any medium, provided the original work is properly cited.

Introduction

Cellular senescence is a state of cell cycle arrest that occurs in response to various stressors, including DNA damage, oxidative stress, and oncogenic signals. This phenomenon, while initially identified in fibroblasts, has been observed in a variety of cell types, including human neural cells (Pawlikowski et al. 2013). The study of senescence in neural contexts is particularly challenging but significant due to its implications in the treatment of neurodegenerative diseases and decline of brain functions during natural aging (Chou et al. 2023). Senescence is characterized by a complex interplay of molecular pathways that lead to the cessation of cell division, changes in cellular morphology, senescence-associated beta-galactosidase activity (SA-beta-gal), upregulation of the key cell cycle regulators such as p21^{Waf1/Cip1} and p16^{Ink4a} and the secretion of pro-inflammatory cytokines, growth factors and proteases collectively known as the senescence-associated secretory phenotype (SASP) (Huang et al. 2022). These changes can have profound effects on the surrounding tissue environment, contributing to both protective and detrimental outcomes.

Recent advances in the field of neurodegenerative diseases have leveraged human neural cell lines to uncover the molecular mechanisms of senescence-related pathways in neurons (Chou et al. 2023). Human neural cell lines such as SH-SY5Y, IMR-32, SK-N-SH, ReNcell VM, LUHMES, and NT2 serve as valuable tools for these studies. Each cell line has unique features, provides a controlled and reproducible model to study the cellular and molecular responses to senescence-inducing stimuli, and is suitable for specific experimental design and research approach. However, conclusions drawn from cellular models have inherent limitations. One of the most popular cellular models for neurobiology research is the SH-SY5Y neuroblastoma cell line. Several studies have utilized SH-SY5Y cells to analyze the senescence response using a variety of methodologies. Tau protein research revealed its role in modulating epigenetic mechanisms of cellular senescence, with markers such as SA-beta-gal and SASP (Magrin et al. 2023). It has been used for the characterization of various agents that modulate the senescence response, including 2,3,7,8-tetrachlorodibenzo-p-dioxin (TCDD), melatonin, frataxin and ebselen (Bolinches-Amorós et al. 2014; Wan et al. 2014; Nopparat et al. 2017; Mukem et al. 2023). In a more mechanistic study, it has been revealed that long intergenic non-coding RNA-p21 (lincRNA-p21) promoted senescence in SH-SY5Y by down-regulating the Wnt/ β -catenin pathway in neurotoxin 1-methyl-4-phenylpyridinium (MPP⁺)-treated cells, increasing p53 and p16^{Ink4} expression (Zhu and Chen 2023). These studies highlight the versatility of SH-SY5Y cells for investigating cellular senescence and potential therapies.

In our study, we focused on the in-depth characterization of senescence-associated changes in two neural model lines, SH-SY5Y and ReNcell VM. Most studies involving ReNcell VM explore their differentiation potential, electrophysiological properties, and use in disease models such as Alzheimer's disease (Donato et al. 2007; Kim et al. 2015; Jorfi et al. 2018). While ReNcell VM cells are frequently used in neurobiological and neurodegenerative studies, there is limited direct research focused specifically on the senescence phenotype in these cells. By employing both classical chromogenic and modern fluorescence-based SA-beta-gal staining, alongside the quantification of DNA damage marker (γ H2A.X foci), changes in nuclear morphology, and levels of cell cycle inhibitors p21^{Waf1/Cip1} and p16^{Ink4a} through qPCR and immunocytochemistry, we are providing a comprehensive analysis of the differences in senescence-associated response in the more frequently used neural cell model SH-SY5Y cells compared to ReNcell VM, which is emerging as a relatively novel model for neurobiological studies.

Materials and Methods

Cell cultivation

The SH-SY5Y cell line (Sigma Aldrich, Cat. No. 94030304) was cultured in Dulbecco's Modified Eagle Medium (DMEM, Gibco, Cat. No. 11960044), supplemented with 2 mM L-glutamine (Gibco, Cat. No. 25030024), 10% heat-inactivated fetal bovine serum (Biosera, Cat. No. FB-1001B/500), and 1% penicillin-streptomycin (Sigma-Aldrich P0781-100ML). Human neural progenitor ReNcell[®] VM (CHEMICON, Cat. No. SCC008) were maintained in culture dishes coated with Matrigel[®] (Corning, Cat. No. 356234). Cells were seeded in ReNcell NSC Maintenance Media (Sigma-Aldrich, Cat. No. SCM005) supplemented with 20 ng/ml fibroblast growth factor-2 (Abcam, Cat. No. ab61845), 20 ng/ml epidermal growth factor (CHEMICON, Cat. No. GF001), and 1% penicillin-streptomycin (Sigma-Aldrich, P0781-100ML). Cells were incubated at 37°C in a humidified atmosphere with 5% CO₂. Senescence was induced by doxorubicin (MPBiomedicals, Cat. No 159101) solution added to the cultivation media of respective cell lines. SH-SY5Y cells were treated with 10 nM and 25 nM doxorubicin (diluted in DMSO) concentrations, and ReNVM cells with 5 nM and 10 nM concentrations for 48 h or 72 h. For the negative controls, the media was mixed with a corresponding amount of DMSO.

SA-beta-gal activity detection

For chromogenic procedure, the media was removed, and cells were washed with 1×PBS before fixation and staining using the SA-beta-gal staining kit (Cell Signaling Tech-

nology, Cat. No. 9860S), according to the manufacturer's instructions. Images were captured under visible light using the Zeiss AxioVert A1 microscope at 20× magnification, equipped with a Zeiss AxioCam 202 mono camera and Zeiss ZEN lite software. Using a fluorescence-based procedure cells were fixed 10 min at RT in 4% paraformaldehyde, centrifuged for 5 min at 250×g, washed with 1% BSA, and centrifuged again 5 min at 250×g. Pellets were then resuspended in a staining working solution, consisting of the CellEvent™ Senescence Green Probe diluted at a 1:2000 ratio in CellEvent™ Senescence Buffer (Invitrogen™, Cat. No. C10840). Staining was performed for 1.5 to 2.0 h in a dry incubator at 37°C without CO₂. Following incubation, cells were centrifuged 5 min at 250×g, and the pellet was washed with 1% BSA followed by another 5 min centrifugation at 250×g. For data evaluation, cells were resuspended in 1×PBS and analyzed *via* flow cytometry. CellEvent™ Senescence Green Flow Cytometry Assay Kit (Invitrogen™, Cat. No. C10840). In order to obtain representative pictures of the CellEvent™ staining, samples were co-stained with Hoechst33258 (Invitrogen, Cat. No. H3569), fixed in mounting media (Sigma-Aldrich, Cat. No. F6057) and imaged at 40× magnification using oil immersion on an LSM 710 confocal microscope (Zeiss, Jena, Germany).

Immunofluorescent staining

After respective treatments, cells were washed with 1×PBS, and fixed in 4% paraformaldehyde for 15 min at RT. Permeabilization was done with 0.1% Triton X-100 for 30 min at RT. Next, cells were incubated with 2% BSA (Sigma-Aldrich, A7906) in 1×PBS for 1 h at RT. Immunostaining was performed with primary antibodies: rabbit anti-p21^{Waf1/Cip1} (Cell Signaling Technology, Cat. No. 2947S), rabbit anti-Histone γ H2A.X (Cell Signaling Technology, Cat. No. 9718T), diluted at a ratio of 1:200 in 0.1% BSA in 1×PBS. This step was conducted overnight at 4°C. A secondary antibody anti-rabbit conjugated with Alexa Fluor 488 (Life Technologies, Cat. No. A21206) diluted 1:1000 in 1% BSA in 1×PBS was applied 1 h at RT. Hoechst33258 (Invitrogen, Cat. No. H3569) in 1×PBS was used for DNA staining. Stained samples were imaged on an LSM 710 confocal microscope (Zeiss, Jena, Germany) at 40× magnification using oil immersion.

RNA isolation, cDNA synthesis and gene expression analysis

RNA was isolated with High Pure RNA Isolation Kit (ROCHE, Cat. No. 11828665001) following the manufacturer's instructions. For cDNA synthesis, 100 ng of total RNA was diluted with nuclease-free water (QIAGEN, Cat. No. 129114) and subsequently used in reverse transcription reaction performed with High Capacity cDNA Reverse

Transcription Kit (Applied Biosystems, Cat. No. 4368814) following the manufacturer's instructions. Gene expression analysis was conducted *via* quantitative real-time PCR (qRT-PCR) in a 10 μ l reaction setup. All samples were analyzed in triplicates for each transcript target in a 96-well plate. Diluted cDNA (20 ng) was mixed with TaqMan probe master mix consisting of 1×TaqMan™ Gene Expression Master Mix (Cat. No. 4369016), 1×TaqMan probe. TaqMan probes Hs04194366_g1, Hs00355782_m1, and Hs00923894_m1 targeting RPL13, p21^{Waf1/Cip1}, and p16^{Ink4a}, mRNA respectively, were purchased from Applied Biosystems. The qRT-PCR analysis was carried out on QuantStudio 6 Flex Real-Time PCR system (Applied Biosystems), following the cycling program: hold at 50°C for 2 min, initial denaturation at 95°C for 10 min, 40 cycles of denaturation at 95°C for 15 s and annealing/extension at 60°C for 1 min. Results were normalized to the expression of RPL13. Data were evaluated using 2^{- $\Delta\Delta$ Ct} method.

Flow cytometry

For data evaluation cells were resuspended in 1×PBS and analyzed on LSRFortessa™ (BD Biosciences) flow cytometry analyzer using a 488 nm laser and 530/30 nm filter. Percentages of SA-beta-gal positive cells were quantified according to the median fluorescence intensity of CellEvent Senescence Green staining in 10,000 probed cells compared to fixed unstained non-treated controls. Data acquisition and analysis was performed in FCS Express 7 software.

Imaging data quantification

For chromogenic SA-beta-gal cell positivity quantification SA-beta-gal activity was quantified using FIJI (ImageJ version 1.54f, Java 1.8.0_322, US National Institutes of Health, Bethesda, Maryland, USA, <https://imagej.net/ij/>, 1997–2018). To correct for uneven illumination, a Gaussian blur was subtracted from each image. The ROIs for individual cells were selected after converting the light-corrected image to 8-bit, auto-thresholding by Huang2, de-noising by de-speckle and median, and watershed. The ROIs were transferred to the blue channel which was deconvoluted (RGB) from the light-corrected image, inverted, and used for white pixel quantification. Data from each image were processed in R (version 4.2.2) (Wickham et al. 2019; R Core Team 2022). The fluorescence intensities of p21^{Waf1/Cip1} and γ H2A.X were quantified using FIJI. The ROIs for individual cells were selected in the Hoechst channel after converting the image to 8-bit, auto-thresholding by Huang2, removing outliers, filling holes, and watershed. The ROIs were transferred to the 8-bit GFP channel and used for pixel quantification. Data from each image were processed in R.

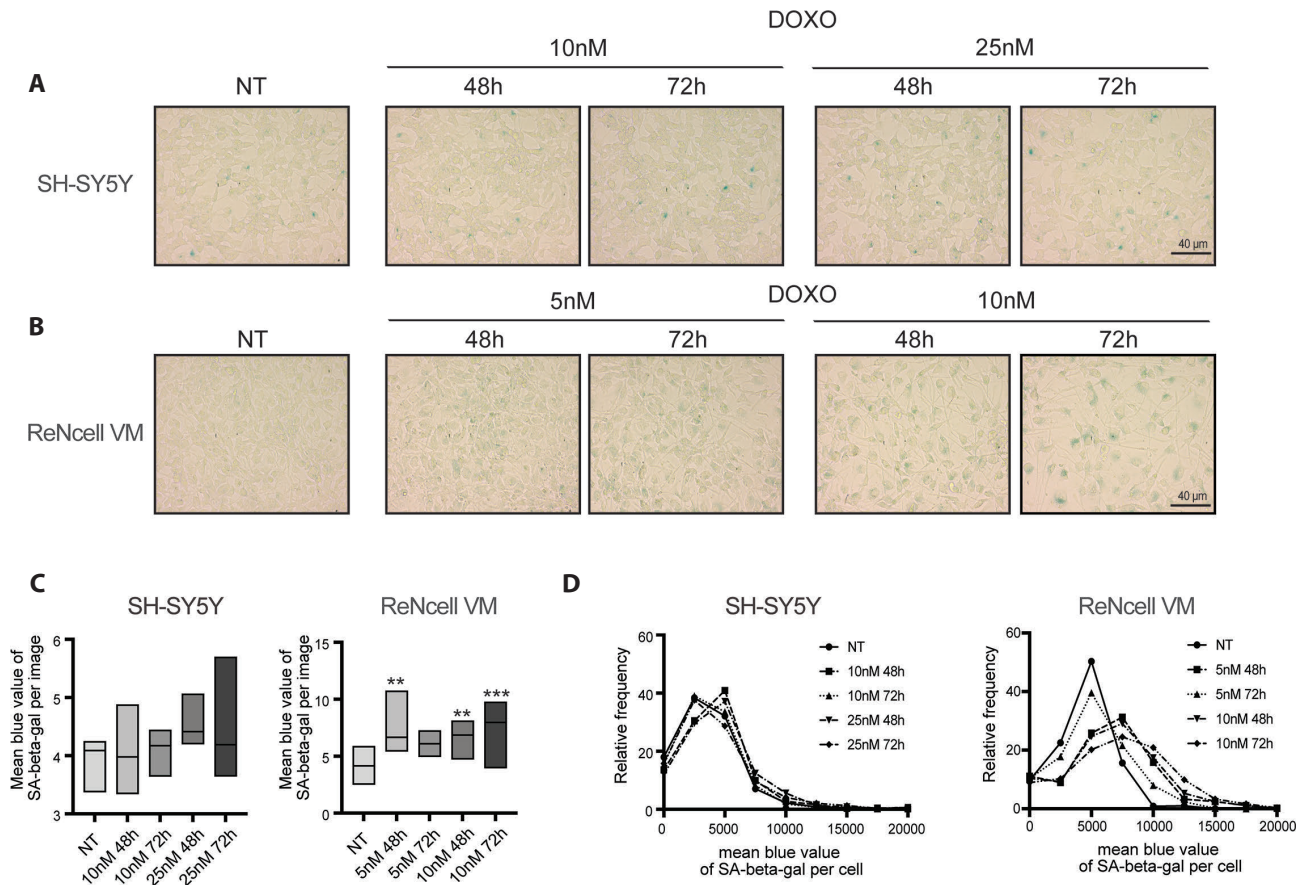


Figure 1. Representative images of chromogenic senescence-associated beta-galactosidase (SA-beta-gal) chromogenic staining in SH-SY5Y cells (A) and ReNcell VM cells (B) after doxorubicin (DOXO) treatments. Cells were treated with DOXO at various concentrations (10, 25 nM or 5, 10 nM) for 48 h and 72 h or remained untreated as controls (NT). SA-beta-gal activity is visualized by blue staining. Scale bars correspond to 40 μ m. C. Quantification of SA-beta-gal staining. Graphs are showing the mean blue values of SA-beta-gal staining *per* image for SH-SY5Y and ReNcell VM under different treatment conditions. Imaging data were quantified using ImageJ. Group comparisons were calculated using the Kruskal-Wallis test with Dunn's correction for multiple comparisons, with ** $p < 0.01$, and *** $p < 0.001$ vs. NT. Central tendency is represented by horizontal median lines. D. Population distribution based on staining intensity. Histograms displaying the relative frequency of mean blue values *per* cell for SA-beta-gal staining in SH-SY5Y and ReNcell VM with indicated treatment conditions. The distribution shifts towards higher staining intensities in treated cells compared to controls corresponds to increased SA-beta-gal activity. (For color figure see online version.)

Statistical analysis

For each experiment, data were collected from three independent repetitions for each condition, and independent collection of samples. For qPCR three replicates for each condition were analyzed in each independent experiment. Group comparisons were calculated using the Kruskal-Wallis test (non-parametric data) with Dunn's correction for multiple comparisons, with nonsignificant $p > 0.05$ and significant * $p < 0.05$, ** $p < 0.01$, and *** $p < 0.001$. For graphical expression of acquired data Prism10 software was used. Results are displayed using box or violin plots and central tendency is represented by horizontal median lines. The frequency distribution data are shown as histograms.

Results

The evaluation of senescence-associated SA-beta-gal activity and changes in cellular morphology in SH-SY5Y and ReNcell VM neural cell lines after doxorubicin treatment

To evaluate the senescence response of SH-SY5Y and ReNcell VM neural cell lines we treated cells with well-described senescence-inducing drug doxorubicin. First, we optimized doxorubicin concentrations based on induced cellular morphology changes and survival rate (data not shown). ReNcell VM cells appeared to be more responsive to senescence induction even in lower concentrations of

doxorubicin compared to SH-SY5Y cells. In order to describe chronic effects (72 h) and possibly subtle differences (48 h) in senescence-associated read-outs between analyzed neural cell lines we continued the experiments with 10 nM and 25 nM doxorubicin concentration for SH-SY5Y and 5 nM and 10 nM doxorubicin for ReNcell VM.

Next, we evaluated the levels of SA-beta-gal activity with two different methods, traditional chromogenic and

novel fluorescence-based assays. Representative images (Figs. 1A,B and 2A,B) show increased SA-beta-gal activity in both SH-SY5Y and ReNcell VM cell lines after doxorubicin treatment. Quantitative analysis of SA-beta-gal staining intensity using ImageJ (Fig. 1C) and flow cytometry (Fig. 2C) provided consistent results. In both approaches, the intensity of SA-beta-gal staining following doxorubicin treatments did not reveal a substantial increase in SH-SY5Y cells while

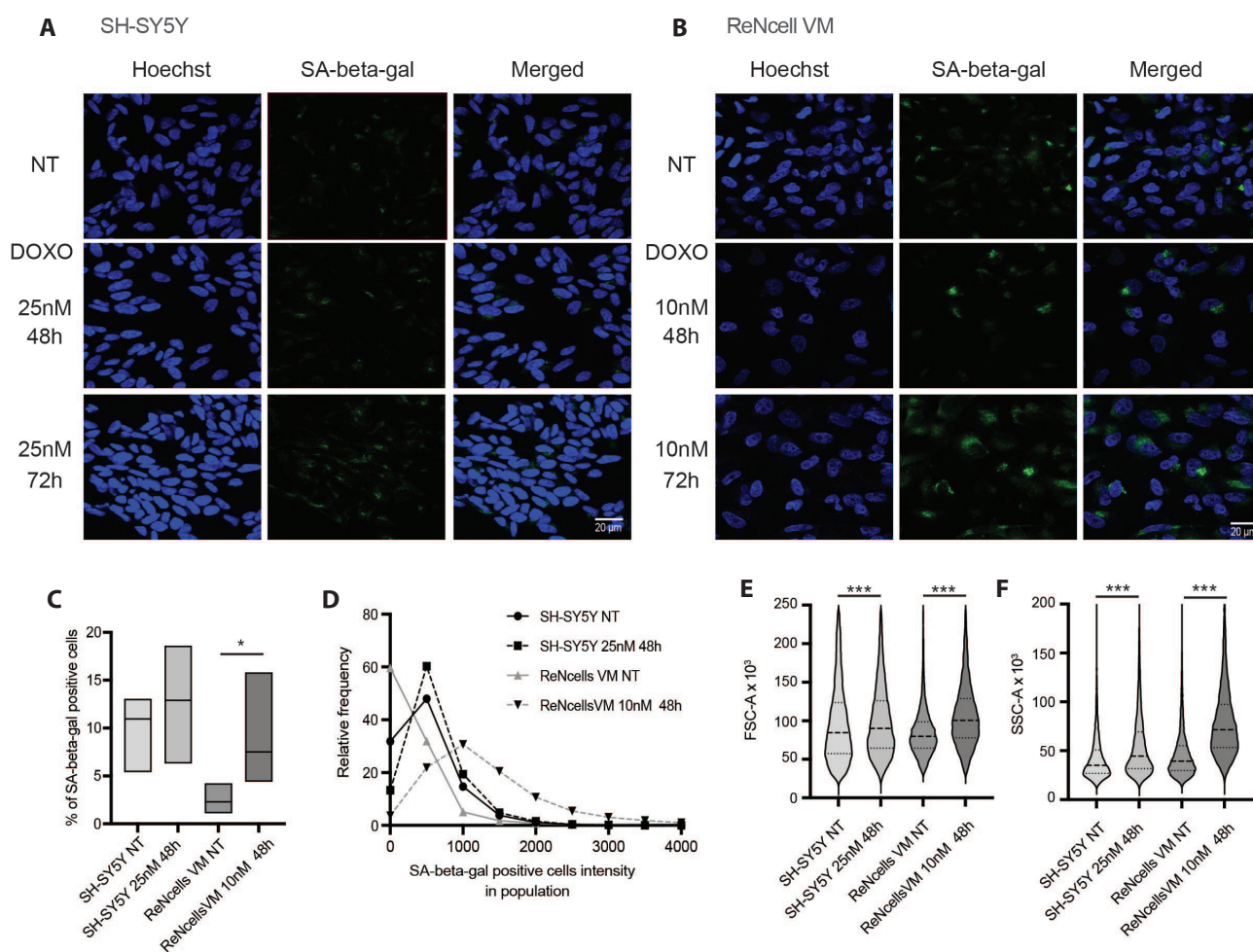


Figure 2. Evaluation of senescence-associated beta-galactosidase (SA-beta-gal) activity together with cell size and granularity in SH-SY5Y and ReNcell VM f cells following doxorubicin (DOXO) treatments and fluorescence-based staining with flow cytometry analysis. **A, B.** Representative images of fluorescence-based SA-beta-gal staining. Cells were treated for 48 h and 72 h with DOXO at 25 nM for SH-SY5Y cells or 10 nM for ReNcell VM cells or remained untreated as controls (NT). SA-beta-gal activity is visualized by green fluorescence, with Hoechst (blue) used for nuclei staining. Scale bars correspond to 20 μ m. **C.** Quantification of SA-beta-gal positive cells by flow cytometry. Box graphs show the percentage of SA-beta-gal positive SH-SY5Y and ReNcell VM cells quantified by flow cytometry under different treatment conditions. **D.** Population distribution based on staining intensity. Histograms displaying the relative frequency of SA-beta-gal positive cells based on fluorescence intensity for SH-SY5Y and ReNcell VM cells. Treatment conditions include 25 nM (for SH-SY5Y cells) or 10 nM (for ReNcell VM cells) DOXO for 48 h. The distribution shifts towards higher intensities in treated cells compared to controls indicate increased SA-beta-gal activity. **E, F.** Evaluation of the cell size and granularity. Violin plots displaying data on cell size and granularity using data recorded by flow cytometer from (E) forward scatter (FSC-A) and (F) side scatter (SSC-A) for SH-SY5Y and ReNcell VM cells populations. Group comparisons were calculated using the Kruskal-Wallis test with Dunn's correction for multiple comparisons, with * $p < 0.05$ and *** $p < 0.001$. Central tendency is represented by horizontal median lines. (For color figure see online version.)

it showed a significant increase in ReNcell VM compared to their respective non-treated controls. Next, we analyzed the distribution of staining intensity across the analyzed cell populations (Figs. 1D, 2D). Histograms of the mean blue values *per cell* for SA-beta-gal staining illustrated in SH-SY5Y cells a slight shift towards higher intensity values after doxorubicin treatment. A more pronounced shift was observed in ReNcell VM suggesting a greater proportion of cells with elevated SA-beta-gal activity. Overall, these results demonstrate that doxorubicin induces significant senescence-related changes in ReNcell VM neural cell line at lower concentrations compared to SH-SY5Y cells.

To quantify differences in cellular morphology we analyzed the flow cytometry data of measures recorded by forward scatter (FSC) and side scatter (SSC) as area values. In both cell lines doxorubicin treatment significantly affected both cell size and granularity as shown by the shift in horizontal median lines and increased spread in the violin plots (Fig. 2E,F).

The comparison of diversity in DNA damage induction and changes in nuclear morphology between SH-SY5Y and ReNcell VM neural cell lines after doxorubicin treatment

To evaluate the DNA damage induced by doxorubicin treatment in SH-SY5Y and ReNcell VM, we analyzed γ H2A.X foci formation using confocal microscopy. Representative images (Fig. 3A,B) show γ H2A.X signals in both cell lines following doxorubicin treatment. Quantitative analysis of the mean fluorescence values of γ H2A.X foci *per cell* showed significant increases in SH-SY5Y as well as ReNcell VM after 72 h of treatment with 25 nM or 10 nM doxorubicin, respectively (Fig. 3C,D).

Data acquired from flow cytometry (Fig. 2C) and quantitative analysis of the mean fluorescence values of γ H2A.X foci (Fig 3C,D) uncovered ongoing changes in cellular and nuclear morphology. Analogously as in the analysis of cell morphology, we displayed the distribution of nuclear sizes in SH-SY5Y and ReNcell VM cells following doxorubicin treatment (Fig. 3E,F). In SH-SY5Y cells, doxorubicin treatment significantly decreased nuclear size after 72 h of treatment (Fig. 3E). ReNcell VM cells showed the opposite trend, with a significant increase in nuclear size after doxorubicin treatment (Fig. 3F).

The analysis of p21^{Waf1/Cip1} and p16^{Ink4a}-mediated response to doxorubicin treatment in SH-SY5Y and ReNcell VM neural cell lines

To further elucidate the senescence response in SH-SY5Y and ReNcell VM neural cell lines after doxorubicin treatment, we analyzed the expression of senescence markers p21^{Waf1/Cip1} and p16^{Ink4a} using qPCR (Fig. 4A,B). The relative mRNA

expression levels of p21^{Waf1/Cip1}, normalized to non-treated controls, increased in both cell lines. However, a significant increase was observed only in ReNcell VM cells after 72 h of treatment with 10 nM doxorubicin. Interestingly, data showed a decrease in relative mRNA expression levels of p16^{Ink4a} in both cell lines with a significant decrease in ReNcell VM treated with 10 nM doxorubicin for 72 h (Fig. 4B).

Representative confocal microscopy images (Fig. 4C,D) showed dynamic changes of p21^{Waf1/Cip1} levels in both SH-SY5Y and ReNcell VM after doxorubicin treatments. Although not significant, the quantification of the mean fluorescence values of p21^{Waf1/Cip1} staining *per cell* showed a gradual increase in SH-SY5Y as a response to doxorubicin treatment followed by its decrease in conditions of 25 nM doxorubicin treatment for 72 h (Fig. 4E). ReNcell VM treated with 10 nM doxorubicin for 48 h showed a significant increase in mean fluorescence values of p21^{Waf1/Cip1} signal compared to non-treated control (Fig. 4F).

Discussion

The specific triggers of neural senescence, the long-term consequences of persisting senescence in the brain, and the potential for therapeutic interventions to modulate senescence in neural cells are currently areas of active investigation. Analyzing these aspects is crucial for developing strategies to mitigate the potential adverse effects of senescence in aging and neurodegenerative diseases (Sikora et al. 2021; Melo Dos Santos et al. 2024). The human-derived neuroblastoma SH-SY5Y cell line has become a popular model widely used in neurobiological research and for investigating neural senescence. Their ability to differentiate into neuron-like cells makes them relevant for studying neural aging and associated diseases. Previous studies conducting senescence-related analyses on SH-SY5Y cells are highly variable.

A study exploring the impact of insulin-like growth factor-binding protein 3 (IGFBP3) in Tau-knockout SH-SY5Y cells revealed that Tau depletion leads to the upregulation of IGFBP3, promoting cellular senescence through epigenetic mechanisms involving the Polycomb repressive complex 2. This study analyzed the levels of IGFBP3, SA-beta-gal activity, p16^{Ink4a}, and lysosomal number and size (Magrin et al. 2023). Another study revealed that TCDD induces premature senescence in SH-SY5Y cells through a reactive oxygen species mechanism, highlighting the role of oxidative stress in activating senescence pathways. This was evidenced by the increased levels of senescence markers such as SA-beta-gal, γ H2A.X foci, p21^{Waf1/Cip1}, p16^{Ink4a}, and F-actin reorganization (Wan et al. 2014). Finally, a research evaluating the role of lincRNA-p21 in MPP⁺-treated SH-SY5Y cells concluded that this non-coding RNA promotes senescence by modulating the Wnt/ β -catenin pathway and increasing oxidative

stress. The senescence markers monitored here include p53, p16^{Ink4a}, telomere length and activity, and levels of reactive oxygen species. Silencing the lincRNA-p21 reversed the

MPP⁺-induced senescence features (Zhu and Chen 2023). Experimental approaches, methods, and read-outs used in the mentioned studies highlight the variety of agents and

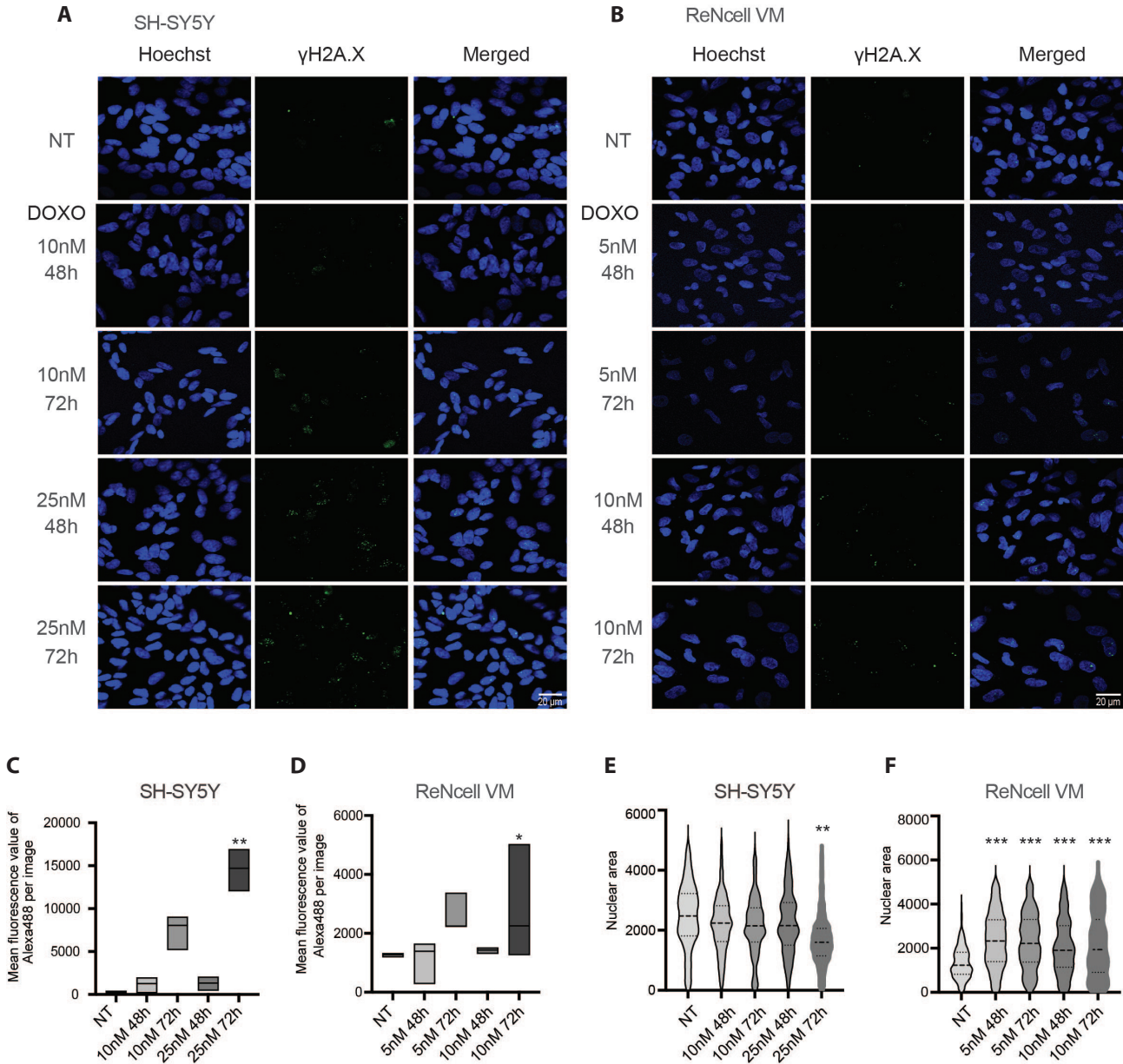
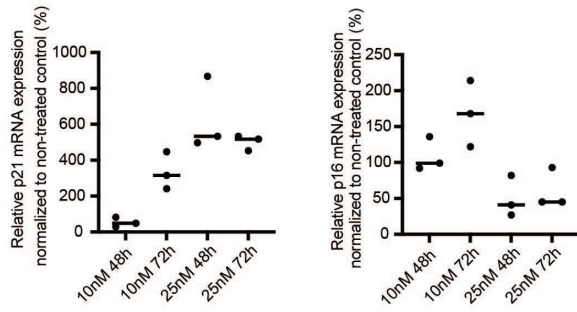
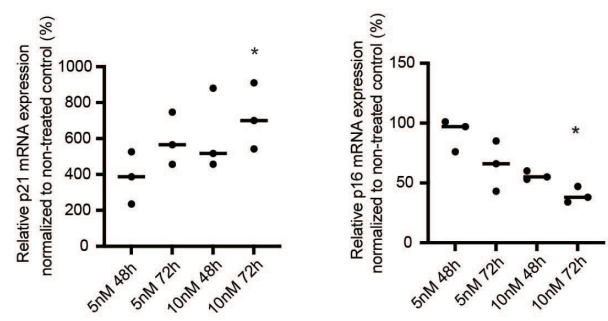


Figure 3. Analysis of γ H2A.X foci and nuclear size in SH-SY5Y and ReNcell VM neural cell lines after doxorubicin (DOXO) treatment. Representative confocal microscopy images showing γ H2A.X foci immunocytochemistry staining in (A) SH-SY5Y and (B) ReNcell VM cells treated with indicated concentrations of DOXO for 48 h and 72 h, as well as untreated controls (NT). γ H2A.X activity is visualized by green fluorescence, with Hoechst used for nuclear staining (blue). Scale bars correspond to 20 μ m. C, D. Quantification of γ H2A.X foci intensity in SH-SY5Y and ReNcell VM cells. Graphs are showing the mean fluorescence values of γ H2A.X staining *per image* for (C) SH-SY5Y and (D) ReNcell VM cells under different treatment conditions. Imaging data were quantified using ImageJ. E, F. Nuclear size distribution in analyzed SH-SY5Y and ReNcell VM populations. Violin plots displaying the distribution of nuclear sizes in (E) SH-SY5Y and (F) ReNcell VM cells after DOXO treatment. Group comparisons were calculated using the Kruskal-Wallis test with Dunn's correction for multiple comparisons, with * $p < 0.05$, ** $p < 0.01$, *** $p < 0.001$ vs. NT. Central tendency is represented by horizontal median lines. (For color figure see online version.)

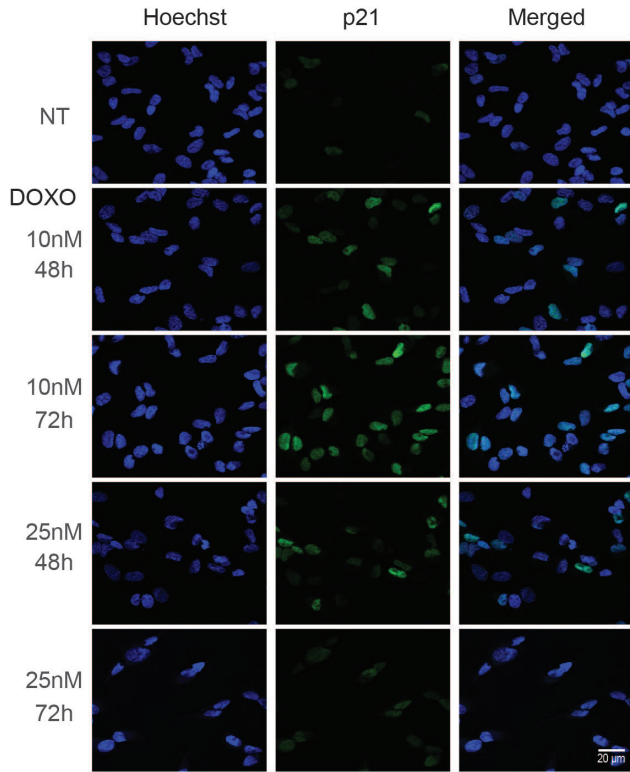
A SH-SY5Y



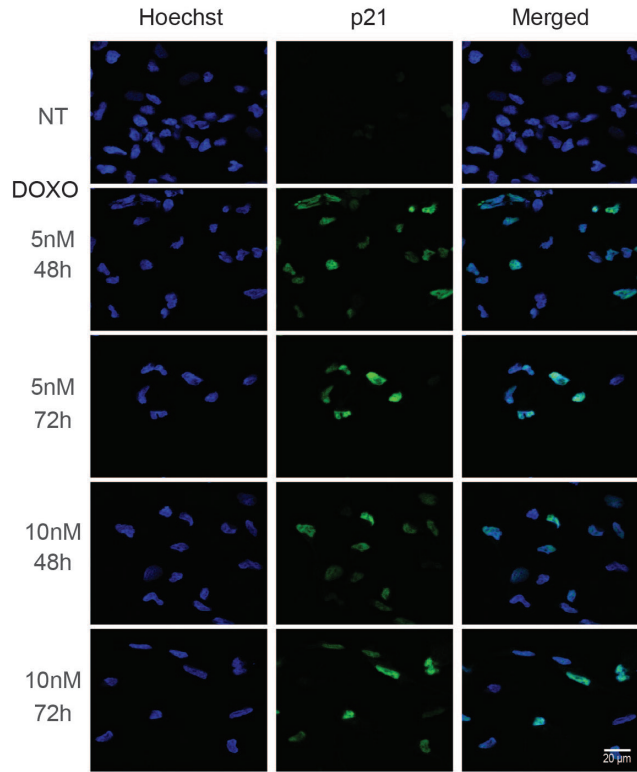
B ReNcell VM



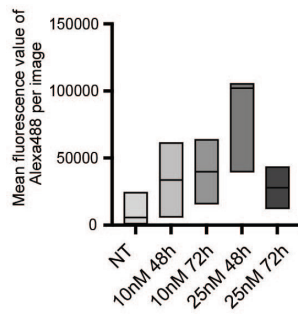
C SH-SY5Y



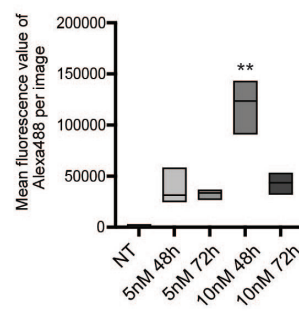
D ReNcell VM



E SH-SY5Y



F ReNcell VM



mechanisms for inducing and investigating cellular senescence in SH-SY5Y cells, reflecting the complexity and multifaceted nature of senescence-related pathways. However, these findings raise questions about the general relevance of these mechanisms to neural senescence, suggesting that the observed responses may be specific to this cell line with limited translation to understanding neural senescence in the brain.

Thus, our study is focused on side-by-side analysis of senescence-associated changes in two neural cell lines which serve as models in various areas of neurobiological research. Besides SH-SY5Y cell line we analyzed the senescence response in ReNcell VM, an immortalized neural progenitor cell line derived from the ventral mesencephalon region of the human fetal brain, which retains a normal diploid karyotype even after prolonged passaging. ReNcell VM cells have been used in neurobiological research for their capacity to differentiate into multiple neural subtypes, including dopaminergic neurons, which is particularly relevant for studies on neurodegenerative diseases such as Parkinson's disease. Studies have shown that ReNcell VM cells can be differentiated into electrophysiologically active neurons capable of firing action potentials and expressing voltage-gated sodium channels (Donato et al. 2007). The ReNcell VM cell line offers a significant advantage over other commonly used cell lines due to its non-cancerous origin, making it particularly suitable for research of the pathological mechanisms and treatment implications of senescence induction in age-related neurodegenerative diseases. Furthermore, its diploid karyotype renders it an attractive tool for subsequent genetic manipulation approaches.

For senescence induction, we selected the widely used chemotherapeutic agent, doxorubicin, which causes persisting DNA damage leading to senescence. It has been shown that doxorubicin-induced DNA damage in SH-SY5Y cells results in persistent DNA damage response activation, contributing to the senescence phenotype. The concentration of doxorubicin used to induce senescence in SH-SY5Y varies, depending on the specific experimental setup and treatment durations. In our study, we aimed to identify a concentra-

tion overlap where doxorubicin induces senescence in both SH-SY5Y and ReNcell VM. We evaluated the concentration range based on observed changes in cellular morphology and survival rates. To capture more subtle differences in early senescence induction (48 h) as well as chronic effects at longer time points (72 h), we selected two treatment concentrations for each cell line; 10 and 25 nM for SH-SY5Y cells, and 5 and 10 nM for ReNcell VM, with a shared overlap at 10 nM. Our results demonstrated that ReNcell VM cells exhibit higher sensitivity to doxorubicin treatments compared to SH-SY5Y cells. This differential response is evident from the lower concentrations of doxorubicin required to induce significant senescence-related changes in ReNcell VM cells. The observed differences may be attributed to intrinsic variations in cellular pathways, drug metabolism, or the baseline expression levels of senescence markers between the two cell lines. Previous studies have shown that different neural cell lines, including SH-SY5Y, exhibit variable drug sensitivities, which could be linked to the neural differentiation stage and specific cellular attributes (Strother et al. 2021). The timing and expression levels of key senescence markers, such as SA-beta-gal, γ H2A.X, p21^{Waf1/Cip1}, and p16^{Ink4a}, varied significantly between SH-SY5Y and ReNcell VM cells. This could be due to differences in the activation of DNA damage response pathways or the efficiency of cell cycle arrest mechanisms. The differential expression of these markers highlights the unique dynamics of senescence in neural models and underscores the importance of evaluating senescence in a cell-type-specific manner (Ogrodnik 2021).

Our study revealed diverse changes and several key features of senescence in these cell lines: (i) we observed aberrant cellular and nuclear morphology, which are the key hallmarks of senescent cells *in vitro*, after doxorubicin treatments in both cell lines. Senescent cells often exhibit an enlarged and flattened shape with increased granularity, which is associated with changes in gene expression, cell function, and metabolism. Additionally, alterations in nuclear morphology can reflect changes in chromatin organization and nuclear structure, which are common aspects of ongoing senescence (Huang et al. 2022). Thus,

◀ **Figure 4.** Analysis of senescence markers p21^{Waf1/Cip1} and p16^{Ink4a} in SH-SY5Y and ReNcell VM neural cell lines after doxorubicin (DOXO) treatment. qPCR Analysis of senescence markers in (A) SH-SY5Y and (B) ReNcell VM cells. Dot plots showing the relative mRNA expression levels of senescence markers p21^{Waf1/Cip1} and p16^{Ink4a}. The expression levels were normalized to RPL13 and presented as fold changes relative to the untreated control. Dots represent three independent experiments, for each was performed independent cell treatment and RNA isolation. Statistical significance was determined using the Kruskal-Wallis test with Dunn's correction for multiple comparisons, with * $p < 0.05$. Central tendency is represented by horizontal median lines. C, D. Representative confocal microscopy images showing p21^{Waf1/Cip1} immunocytochemistry staining in (C) SH-SY5Y and (D) ReNcell VM p21^{Waf1/Cip1} cells is visualized by green fluorescence, with Hoechst used for nuclear staining (blue). Scale bars correspond to 20 μ m. E, F. Quantification of p21^{Waf1/Cip1} intensity in SH-SY5Y and ReNcell VM cells. Graphs are showing the mean fluorescence values of p21^{Waf1/Cip1} staining *per* image for (E) SH-SY5Y and (F) ReNcell VM cells under different treatment conditions. Imaging data were quantified using ImageJ. Group comparisons were calculated using the Kruskal-Wallis test with Dunn's correction for multiple comparisons, with ** $p < 0.01$ vs. NT. Central tendency is represented by horizontal median lines. (For color figure see online version.)

assessing these parameters provides a more comprehensive evaluation of the senescence-associated read-outs and helps to validate the findings from diverse molecular markers such as SA-beta-gal activity, p21^{Waf1/Cip1}, and p16^{Ink4a}. (ii) The quantification of SA-beta-gal staining revealed relatively high basal SA-beta-gal activity in SH-SY5Y cell line (especially using the fluorescent method) compared to ReNcell VM leading to relative absence of significance in the SA-beta-gal staining increase. This effect might not be captured by other studies using higher concentrations of doxorubicin. In comparison, the increase in SA-beta-gal activity evaluated by both methods was significant in ReNcell VM. (iii) Our results revealed that DNA damage was more prominent in SH-SY5Y cells compared to ReNcell VM cells, as evidenced by the quantification of γ H2A.X signals. Specifically, SH-SY5Y cells exhibited γ H2A.X foci intensity of around 15,000, whereas the maximum intensity in ReNcell VM cells reached 5,000. This significant difference suggests that SH-SY5Y cells experience more extensive DNA damage upon doxorubicin treatment. Possible explanations for this observation could be the inherent differences in the DNA repair mechanisms, the susceptibility to doxorubicin-induced DNA damage, or the polyploid nature of neuroblastoma cells, which further amplifies the detected signal due to the increased number of formed DNA damage foci. Upregulation of γ H2A.X in SH-SY5Y cells indicates a robust activation of the DNA damage response pathway, which is a critical aspect of senescence induction. (iv) In contrast to the DNA damage response, p21^{Waf1/Cip1} expression was stronger in ReNcell VM cells compared to SH-SY5Y cells under the same conditions. The intensity of p21^{Waf1/Cip1} staining reached around 150,000 in ReNcell VM cells, while it was approximately 100,000 in SH-SY5Y cells. Since p21^{Waf1/Cip1} is a key regulator of cell cycle arrest during senescence, its higher expression in ReNcell VM cells suggests a more pronounced activation of senescence through this pathway. The differential expression may be attributed to variations in the signalling pathways that regulate p21^{Waf1/Cip1} transcription and stability. Stronger p21^{Waf1/Cip1} response in ReNcell VM cells highlights their increased sensitivity to doxorubicin-induced senescence, which is consistent with the observed lower threshold for senescence induction in these cells. (v) Interestingly, our study also revealed a decreasing trend in p16^{Ink4a} levels following doxorubicin treatments. This observation was unexpected, as p16^{Ink4a} is often involved in the later stages of the senescence process. One possible explanation for the downregulation could be related to the specific regulatory mechanisms in neural cells. It is known that p16^{Ink4a} expression can be influenced by various factors, including epigenetic modifications, transcriptional regulation, and protein stability. In the context of neural cells, it is possible that compensatory mechanisms or feedback loops are in place to modulate p16^{Ink4a} levels during senescence. In ad-

dition, the interplay between p16^{Ink4a} and other cell cycle regulators, such as p21^{Waf1/Cip1}, might contribute to the observed decrease. Notably, a study by Verma et al. (2021) on the effects of α -synuclein preformed fibrils in Parkinson's disease models found that p16^{Ink4a} levels can decrease in certain contexts of cellular stress and senescence initiation, suggesting complex regulation mechanisms in neural cells. Further investigation is needed to elucidate the precise mechanisms underlying this phenomenon and its implications for neural cell senescence.

The findings from this study have important implications for utilizing SH-SY5Y and ReNcell VM cells as models in neural senescence research. Our results suggest that ReNcell VM cells, which are not frequently used for senescence studies, may provide a more sensitive model for studying senescence-related changes in neural cells (Kim et al. 2015; Jorfi et al. 2018). Although this study provides valuable insights regarding differential senescence dynamics in SH-SY5Y and ReNcell VM cells, several limitations including the choice of inducing stimulus (e.g. bleomycin), selected markers, or analytical methods should be considered. Additionally, it is important to further investigate the downstream effectors of neural senescence including components of SASP.

The differential senescence responses observed in SH-SY5Y and ReNcell VM cells may have significant implications for understanding the role of senescence in neurodegenerative diseases. Senescent cells accumulate in the nervous system with aging and neurodegenerative conditions, contributing to disease progression. Our findings suggest that ReNcell VM could serve as a more relevant model for studying the mechanisms of senescence in neurodegenerative diseases, potentially leading to the identification of novel therapeutic targets (Kritsilis et al. 2018; Si et al. 2021). The development of senolytic therapies, which selectively eliminate senescent cells, holds promise for treating age-related neurodegenerative disorders (Ribierre et al. 2024). Our study provides a foundation for evaluating the efficacy of senolytic drugs in neural cell models. The higher sensitivity of ReNcell VM cells to senescence induction suggests that they may be particularly useful for screening senolytic compounds.

Conflicts of interest. The authors declare that there are no conflicts of interest regarding the publication of this paper. This research was not sponsored by another person or entity with which the researchers have other affiliation or a financial involvement than stated.

Acknowledgements. This project was supported by Slovak research and development agency (No. APVV-20-0331), International centre for genetic engineering and biotechnology (ICGEB CRP/SVK22-04_EC) and Scientific grant agency of the Ministry of Education of the Slovak Republic and Slovak Academy of Sciences VEGA2/0158/21. DF and DN were financially supported by European Union's Horizon 2020 research and innovation programme on the basis of a grant agreement under the Marie Skłodowska-Curie

funding scheme No. 945478; by the Slovak Academic and Scientific Programme No. 1085/01/02 (DF) and No. 3333/03/02 (DN).

Author contributions. Conceptualization, KM, DF; methodology, KM, DM, LF, DN, DF; formal analysis, KM, DN, DF; investigation, KM, DF; writing – original draft preparation, DF; writing – review and editing, KM, DM, LF, DN, DF; supervision, project administration funding acquisition, DF.

References

- Bolinches-Amorós A, Mollá B, Pla-Martín D, Palau F, González-Cabo P (2014): Mitochondrial dysfunction induced by frataxin deficiency is associated with cellular senescence and abnormal calcium metabolism. *Front. Cell. Neurosci.* **8**, 124
<https://doi.org/10.3389/fncel.2014.00124>
- Chou S-M, Yen YH, Yuan F, Zhang SC, Chong CM (2023): Neuronal senescence in the aged brain. *Aging Dis.* **14**, 1618-1632
<https://doi.org/10.14336/AD.2023.0214>
- Donato R, Miljan EA, Hines SJ, Aouabdi S, Pollock K, Patel S, Edwards FA, Sinden JD (2007): Differential development of neuronal physiological responsiveness in two human neural stem cell lines, *BMC Neurosci.* **8**, 36
<https://doi.org/10.1186/1471-2202-8-36>
- Huang W, Hickson LJ, Eirin A, Kirkland JL, Lerman LO (2022): Cellular senescence: the good, the bad and the unknown. *Nat. Rev. Nephrol.* **18**, 611-627
<https://doi.org/10.1038/s41581-022-00601-z>
- Jorfi M, D'Avanzo C, Tanzi RE, Kim DY, Irimia D (2018): Human neurospheroid arrays for in vitro studies of Alzheimers disease. *Sci. Rep.* **8**, 2450
<https://doi.org/10.1038/s41598-018-20436-8>
- Kim YH, Choi SH, D'Avanzo C, Hebisch M, Sliwinski C, Bylykbashi E, Washicosky KJ, Klee JB, Brüstle O, Tanzi RE, Kim DY (2015): A 3D human neural cell culture system for modeling Alzheimers disease. *Nat. Protoc.* **10**, 985-1006
<https://doi.org/10.1038/nprot.2015.065>
- Kritsilis M, V Rizou S, Koutsoudaki PN, Evangelou K, Gorgoulis VG, Papadopoulos D (2018): Ageing, cellular senescence and neurodegenerative disease. *Int. J. Mol. Sci.* **19**, 2937
<https://doi.org/10.3390/ijms19102937>
- Magrin C, Bellafante M, Sola M, Piovesana E, Bolis M, Cascione L, Napoli S, Rinaldi A, Papin S, Paganetti P (2023): Tau protein modulates an epigenetic mechanism of cellular senescence in human SH-SY5Y neuroblastoma cells. *Front. Cell Dev. Biol.* **11**, 1232963
<https://doi.org/10.3389/fcell.2023.1232963>
- Melo Dos Santos LS, Trombetta-Lima M, Eggen B, Demaria M (2024): Cellular senescence in brain aging and neurodegeneration. *Ageing Res. Rev.* **93**, 102141
<https://doi.org/10.1016/j.arr.2023.102141>
- Mukem S, Sayoh I, Maungchanburi S, Thongbuakaew T (2023): Ebselen, iron uptake inhibitor, alleviates iron overload-induced senescence-like neuronal cells SH-SY5Y via suppressing the mTORC1 signaling pathway. *Adv. Pharmacol. Pharm. Sci.* **2023**, 6641347
<https://doi.org/10.1155/2023/6641347>
- Nopparat C, Sinjanakhom P, Govitrapong P (2017): Melatonin reverses H2 O2 -induced senescence in SH-SY5Y cells by enhancing autophagy via sirtuin 1 deacetylation of the RelA/p65 subunit of NF-κB. *J. Pineal Res.* **63**, e12407
<https://doi.org/10.1111/jpi.12407>
- Ogrodnik M (2021): Cellular aging beyond cellular senescence: Markers of senescence prior to cell cycle arrest in vitro and in vivo. *Aging Cell* **20**, e13338
<https://doi.org/10.1111/acer.13338>
- Pawlikowski JS, Adams PD, Nelson DM (2013): Senescence at a glance. *J. Cell Sci.* **126**, 4061-4067
<https://doi.org/10.1242/jcs.109728>
- R Core Team (2022): R: A language and environment for statistical computing. R Foundation for Statistical Computing, Vienna, Austria. <https://www.R-project.org/>.
- Ribierre T, Bacq A, Donneger F, Doladilhe M, Maletic M, Roussel D, Le Roux I, Chassoux F, Devaux B, Adle-Biassette H, et al. (2024): Targeting pathological cells with senolytic drugs reduces seizures in neurodevelopmental mTOR-related epilepsy. *Nat. Neurosci.* **27**, 1125-1136
<https://doi.org/10.1038/s41593-024-01634-2>
- Si Z, Sun L, Wang X (2021): Evidence and perspectives of cell senescence in neurodegenerative diseases. *Biomed. Pharmacother.* **137**, 111327
<https://doi.org/10.1016/j.biopha.2021.111327>
- Sikora E, Bielak-Zmijewska A, Dudkowska M, Krzystyniak A, Mosieniak G, Wesierska M, Włodarczyk J (2021): Cellular senescence in brain aging. *Front. Aging Neurosci.* **13**, 646924
<https://doi.org/10.3389/fnagi.2021.646924>
- Strother L, Miles GB, Holiday AR, Cheng Y, Doherty GH (2021): Long-term culture of SH-SY5Y neuroblastoma cells in the absence of neurotrophins: A novel model of neuronal ageing. *J. Neurosci. Methods* **362**, 109301
<https://doi.org/10.1016/j.jneumeth.2021.109301>
- Verma DK, Seo BA, Ghosh A, Ma SX, Hernandez-Quijada K, Andersen JK, Ko HS, Kim YH (2021): Alpha-synuclein preformed fibrils induce cellular senescence in Parkinsons disease models. *Cells* **10**, 1694
<https://doi.org/10.3390/cells10071694>
- Wan C, Liu J, Nie X, Zhao J, Zhou S, Duan Z, Tang C, Liang L, Xu G (2014): 2,3,7,8-Tetrachlorodibenzo-P-dioxin (TCDD) induces premature senescence in human and rodent neuronal cells via ROS-dependent mechanisms. *PLoS One* **9**, e89811
<https://doi.org/10.1371/journal.pone.0089811>
- Wickham H, Averick M, Bryan J, Chang W, McGowan LD, François R, Grolemund G, Hayes A, Henry L, Hester J, et al. (2019): Welcome to the tidyverse. *JOSS* **4**, 1686
<https://doi.org/10.21105/joss.01686>
- Zhu J, Chen L (2023): LincRNA-p21 promotes cellular senescence by down-regulating the Wnt/β-catenin pathway in MPP+-treated SH-SY5Y cells. *Comb. Chem. High Throughput Screen.* **26**, 2476-2486
<https://doi.org/10.2174/1386207326666230417103137>

Received: June 4, 2024

Final version accepted: June 11, 2024